

Polarization agnostic continuous variable quantum key distribution

Brian P. Williams*¹ and Nicholas A. Peters¹

¹Quantum Information Science Section, Oak Ridge National Laboratory, Oak Ridge, Tennessee USA 37831*

We introduce a polarization agnostic method for Gaussian-modulated coherent state (GCMS) continuous-variable quantum key distribution (CVQKD). Due to the random and continuous nature of the GCMS protocol, Alice, the transmitter, can encode two distinct quadratures in each of two orthogonal polarization modes, such that Bob, the receiver, measures valid GCMS quadratures in a single polarization mode even when polarization changes occur during transmission. This method does not require polarization correction in the optical domain, does not require monitoring both polarization modes, reduces loss by eliminating optical components, and avoids the noise injected by polarization correction algorithms.

Continuous variable quantum key distribution (CVQKD) based on optical coherent detection is a promising alternative to discrete photon methods due to its use of common telecom components, room temperature operation, ability to coexist with telecom traffic [1–3], and advancing implementations with photonic integrated circuits [4–6]. The well-established Gaussian-modulated coherent state (GMCS) protocol [7] has the most robust proven security and has been demonstrated over 200 km of fiber [8]. One technical challenge in CVQKD is to correct the polarization at the receiver such that the signal is aligned with Bob’s local oscillator (LO), his reference laser used for homodyne measurement. When the polarization states of the signal and LO are not aligned Bob’s signal-to-noise ratio is reduced. This reduction has a critical impact on the secret-key rate and achievable transmission distance.

Polarization correction and management strategies in CVQKD consist of passive and active methods. Polarization diverse receivers can be used to passively monitor both polarization modes [9–13] at the cost of additional detector resources. Active methods utilize a polarization controller and ancillary signal feedback to align the signal and LO [3, 14–16]. The reduction of detector resources achieved using active methods requires the addition of more complex optical modulation and real-time data processing.

In this article we present the first, to our knowledge, passive approach for GMCS CVQKD polarization management that does not require monitoring both polarizations at the receiver. Briefly, our Alice encodes independent GMCS signals in each of two orthogonal polarizations. These encoded values undergo a polarization transformation in the optical fiber but remain valid GMCS signals. Given that Alice can identify the polarization transformation post-transmission, Alice can digitally transform her stored encoding values such that correlations with Bob are recovered as seen in Fig. 1. Our method only requires monitoring of one polarization, eliminates the cost and loss associated with polarization

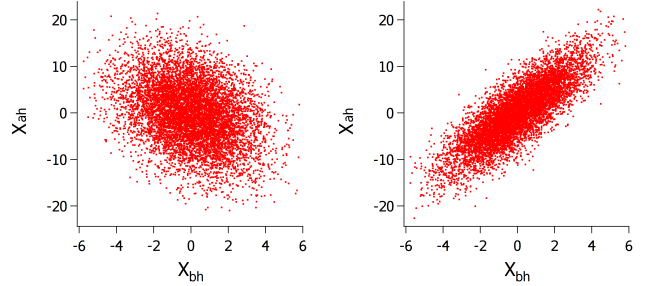


FIG. 1. Bob’s X_{bh} versus Alice’s sent signal X_{ah} . Left) without corrections to Alice’s encoding and Right) with corrections. Alice sends a GMCS signal with average photon number $\langle n \rangle = 5$, $V_A = 10$. The polarization parameters recovered from this data are $\phi = 2.28$, $\delta = -0.05$, $\theta = 0.84$.

control components, and avoids noise injected by polarization correction algorithms.

I. GMCS CV-QKD

The fundamental make-up of a CV-QKD system is a coherent communications system [17, 18]. A weak signal, about one photon, is transmitted from Alice to Bob. Bob interferes this weak signal with a bright reference laser, the LO. This interference results in an amplification of the signal and allows a phase measurement relative to Bob’s LO. Bob’s measurement is often carried out using dual-quadrature homodyne detection which outputs two measurements, the quadratures X and P [19]. The values X and P form the raw-key between Alice and Bob which feeds the reconciliation process to produce the final secret key.

A typical GMCS CVQKD protocol is carried out in the following steps:

1. Alice picks random quadrature values X_a and P_a from a common Gaussian distribution with variance V_A in shot-noise units (SNU).
2. Alice encodes X_a and P_a , in $\sqrt{SN\bar{U}}$, onto a light pulse which is equivalent to picking an average pho-

* williamsbp@ornl.gov

ton number and phase.

3. Alice transmits the encoded light pulse to Bob in a single-polarization through single-mode optical fiber in which polarization transformations occur.
4. Bob receives Alice's light signal. Bob corrects the polarization using active devices before detection. Alternatively, Bob can use a polarization diverse receiver to make quadrature measurements.
5. Steps 1-5 are repeated to complete a *packet*. In our case 7.8k pulses are sent with 1 μ s between pulses, 1 Mhz.
6. Bob sends Alice a fraction of his results which are utilized to estimate the transmission T for the optical link and the excess noise ξ both of which impact the final secret-key rate.
7. Alice and Bob generate a secret-key through a reconciliation protocol.

The performance metrics for GMCS involve the variance of Bob's measurements and Alice's encodings for each quadrature. These variances are normalized to the measured quadrature shot-noise and given in SNU. The shot-noise is the variance due to the presence of the LO. It is typically measured, in part, by blocking light entering the signal port of the detector. Bob's measured variance, in our experiment calculated for a single received packet, is given as

$$V_B = \frac{\eta T}{2} (V_A + \xi) + 1 + \epsilon \quad (1)$$

where V_A is Alice's single quadrature modulation variance, ξ is the excess noise assumed to be contributed by Eve, η is the efficiency of Bob's detector, T is the optical link transmission, the $\frac{1}{2}$ fraction results from the dual-quadrature homodyne detection, the "1" term represents the shot-noise, and ϵ is the detector noise. Again, the variance quantities are all in SNU.

II. POLARIZATION AGNOSTIC ENCODING FOR GMCS CVQKD

For the GMCS protocol, Alice independently samples values to encode quadratures X, P from a common Gaussian distribution

$$f(q) = \frac{1}{\sqrt{2\pi V_A}} e^{-\frac{q^2}{2V_A}} \quad (2)$$

where $q \in \{X, P\}$.

Given sampled X, P values, Alice's prepared signal can be written as the coherent state [20]

$$|\alpha\rangle = \hat{D}(\alpha)|0\rangle = e^{\alpha\hat{a}^\dagger - \alpha^*\hat{a}}|0\rangle \quad (3)$$

where the creation and annihilation operators have the property $[\hat{a}, \hat{a}^\dagger] = 1$ and

$$\alpha = |\alpha| \cos \gamma + i |\alpha| \sin \gamma = X + iP. \quad (4)$$

Using Jones polarization notation, Alice's state prepared in horizontal polarization can be written as

$$|\alpha_H, 0\rangle = \begin{bmatrix} \alpha_h \\ 0 \end{bmatrix} = \begin{bmatrix} X_h + iP_h \\ 0 \end{bmatrix}. \quad (5)$$

We note that this representation is a departure from some CVQKD literature where the components of the column vector are the quadratures X, P and the polarization is assumed to be single-mode.

Due to the birefringent nature of standard single mode optical fiber, light transmitted through such fiber results in changes to the light polarization. It is shown in [21] that the many polarization rotations and phase changes accumulated in a single-mode fiber transmission are equivalent to a single rotation

$$R(\theta) = \begin{bmatrix} \cos \theta & -\sin \theta \\ \sin \theta & \cos \theta \end{bmatrix} \quad (6)$$

and single phase change

$$C(\delta) = \begin{bmatrix} e^{i\frac{\delta}{2}} & 0 \\ 0 & e^{-i\frac{\delta}{2}} \end{bmatrix} \quad (7)$$

given here as Jones matrices [22].

In the case of CVQKD, a relative phase also exists between the LO and Alice's signal. This phase can be included as an additional global phase

$$G(\phi) = \begin{bmatrix} e^{i\phi} & 0 \\ 0 & e^{i\phi} \end{bmatrix}. \quad (8)$$

Now, assume that Alice encodes independent quadratures in each polarization, all from a common Gaussian distribution. We can write a single instance of this encoding as

$$|\alpha_H, \beta_V\rangle = \begin{bmatrix} X_{ah} + iP_{ah} \\ X_{av} + iP_{av} \end{bmatrix} \quad (9)$$

where α and β describe the horizontal and vertical polarization coherent states, respectively.

The transformed state after propagating through a single-mode optical fiber is

$$R(\theta) G(\phi) C(\delta) |\alpha_H, \beta_V\rangle = \begin{bmatrix} X_{bh} + iP_{bh} \\ X_{bv} + iP_{bv} \end{bmatrix} \quad (10)$$

where $X_{bh}, P_{bh}, X_{bv},$ and P_{bv} depend on $X_{ah}, P_{ah}, X_{av},$ and $P_{av},$ for instance

$$\begin{aligned} X_{bh} = & \left[X_{ah} \cos\left(\phi + \frac{\delta}{2}\right) - P_{ah} \sin\left(\phi + \frac{\delta}{2}\right) \right] \cos \theta \\ & - \left[X_{av} \cos\left(\phi - \frac{\delta}{2}\right) - P_{av} \sin\left(\phi - \frac{\delta}{2}\right) \right] \sin \theta. \end{aligned} \quad (11)$$

Bob's quadratures P_{bh} , X_{bv} , and P_{bv} have similar forms.

Given that we rewrite X_{ah} , P_{ah} , X_{av} , and P_{av} as functions of X_{bh} , P_{bh} , X_{bv} , and P_{bv} using Eq. 2 and 10, we can determine the X_{bv} quadrature distribution by integrating over Bob's remaining quadratures P_{bh} , X_{bv} , P_{bv} [23]

$$F(X_{bh}) = \int \int \int dP_{bh} dX_{bv} dP_{bv} \times f(X_{ah}) \times f(P_{ah}) \times f(X_{av}) \times f(P_{av}). \quad (12)$$

Alternative to solving Eq. 10, it may be verified that

$$X_{ah}^2 + P_{ah}^2 + X_{av}^2 + P_{av}^2 = X_{bh}^2 + P_{bh}^2 + X_{bv}^2 + P_{bv}^2 \quad (13)$$

such that

$$\begin{aligned} F(X_{bh}) &= \int \int \int dP_{bh} dX_{bv} dP_{bv} \\ &\times f(X_{bh}) \times f(P_{bh}) \times f(X_{bv}) \times f(P_{bv}) \\ &= f(X_{bh}) \end{aligned} \quad (14)$$

resulting in the quadrature X_{bh} having the same Gaussian distribution as Alice's original quadratures given in Eq. 2. Clearly, Bob's other quadratures P_{bh} , X_{bv} , and P_{bv} also have this common Gaussian distribution. Above we have neglected loss and efficiency terms which will reduce the value of Bob's measured quadratures. This does not impact our result.

Since polarization transformations result in Bob's quadratures being a combination of Alice's encoded quadratures, it seems plausible that there would be correlations in Bob's measurements. The calculation in Eq. 14 already supports quadrature independence, however for example, it can also be verified that

$$\begin{aligned} &\langle (X_{bh} - X_{bv})^2 \rangle \\ &= \int \int \int \int dX_{ah} dP_{ah} dX_{av} dP_{av} \\ &\times f(X_{ah}) \times f(P_{ah}) \times f(X_{av}) \times f(P_{av}) \\ &\times (X_{bh} - X_{bv})^2 = 2V_A \end{aligned} \quad (15)$$

where X_{bh} , X_{bv} are functions of X_{ah} , P_{ah} , X_{av} , and P_{av} . This shows that no correlations exist between Bob's horizontal X_{bh} and vertical X_{bv} quadratures. The variance is just the sum of the individual Gaussian distributions. If there was a correlation, we would expect a reduction in this value. This same relation holds for any combination of the quadratures. Thus, there are no correlations between Alice's transformed quadratures or Bob's measured quadratures, which allows them to be treated as independent GMCS channels. As an example, we plot Alice's transformed values X_{ah} versus X_{av} in Fig. 2 from the experiment given in Fig. 1. As expected, no correlations appear.

If Alice can determine with sufficient accuracy the polarization rotation and phase parameters θ , ϕ , and δ from Bob's shared data, she can digitally transform her

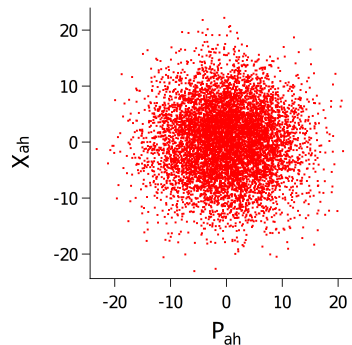


FIG. 2. Here we plot Alice's transformed values X_{ah} and P_{ah} to show that no correlations exist between transformed quadratures.

recorded encoding values to match the optical polarization transformation with the transform given in Eq. 10. The final result will be as if Alice had originally encoded these quadrature values and no polarization changes occurred in the optical fiber link during transmission. It is not the case that Bob can correct his own dataset when using a single DQHD, since he does not have data from the unmonitored polarization.

Parameter estimation for the channel transmission T and excess noise ξ is a necessary step in the CVQKD protocol since they impact the achievable secret key-rate. As we will show, this same dataset can be used concurrently to determine the effective polarization parameters present in the signal received from Alice.

Our modified polarization agnostic CVQKD protocol is:

1. Alice picks random quadrature values X_{ah} , P_{ah} , X_{av} , and P_{av} from a common Gaussian distribution with variance V_A .
2. Alice encodes X_{ah} , P_{ah} on the horizontal and X_{av} , P_{av} on the vertical polarization components of her light pulse.
3. Alice transmits the encoded light pulse to Bob in a single-mode optical fiber in which polarization transformations occur.
4. Bob receives Alice's light signal and measures his own quadrature values X_{bh} , P_{bh} in a single polarization.
5. Steps 1-5 are repeated to complete a *packet*. In our case 7.8k pulses are sent with a 1 μ s repetition rate, 1 Mhz.
6. Bob sends Alice a fraction of his results which are utilized to estimate the transmission T for the optical link, the excess noise ξ , and the polarization parameters θ , ϕ , and δ .
7. Alice rotates her stored quadratures digitally using estimates for θ , ϕ , and δ .

8. Alice and Bob generate a secret-key through a reconciliation protocol.

III. EXPERIMENT

One possible implementation of Alice’s transmitter is seen in Fig. 3 which utilizes parallel paths and four modulators to carry out encodings of all four quadratures. This transmitter is conceptually simple to understand and has the equivalent outcome as our method detailed below.

To avoid the need to use four modulators, we implemented the transmitter seen in Fig. 4 which utilizes time-multiplexing and a bias-free phase-amplitude modulator [3, 24–26] to encode each polarization’s quadratures with a single LiNbO₃ waveguide phase modulator (EOSpace). Referencing Fig. 4, a single frequency-stabilized continuous wave (CW) laser (OE Waves OE4028) generates 1542 nm light which is split using a 90:10 into the encoding and LO paths. The final CW LO power is 8.7 mW. In the encoding path, Alice utilizes a LiNbO₃ waveguide amplitude modulator (EOSpace) to generate 10 ns-wide pulses at a 1 MHz repetition rate. After passing through a circulator (1→2), a half-wave plate allows balancing of the light amplitude entering the horizontal and vertical polarization paths. The upper vertical path delays by 200 ns. The lower horizontal path has no delay but rotates the polarization from horizontal to vertical such that all encoded light travels the same optical path in the delay lines and phase-amplitude modulator. A phase modulator is placed asymmetrically in the Sagnac loop such that distinct phases can be applied to clockwise and counter-clockwise propagating pulses with a 100 ns delay between them [3]. The encoded pulses ultimately exit the Sagnac loop along different delay paths than they entered removing the time delay between the different polarizations (overlapping them in time). The encoded signal passes through the amplitude balancing HWP again which results in a change to the polarization state. This can be assumed to be part of the overall polarization transformation in the transmission link. After passing through the circulator (2→3), a constant attenuation is applied to adjust the overall amplitude range before being sent to Bob.

Alice utilizes the transmitter in Fig. 4 to generate packets containing 7.8k 10-ns pulses with GMCS encodings in Alice’s horizontal and vertical polarizations, 31.2k quadrature values per packet in total. A random polarization transformation is selected and applied to all the pulses in a single packet as seen at left in Fig. 5. We utilized a Luna PCD-M02 dynamic polarization controller to implement the polarization transformation. A unique random polarization transformation was applied to each packet. The packets contain 7.8k pulses at 1 μ s repetition rate, making the packet duration 7.8 ms. From the literature, a selection of reported polarization stability time durations range from μ s for coiled fiber in a high

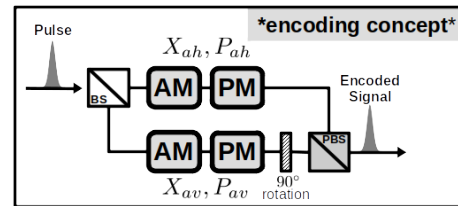


FIG. 3. Alice could encode each polarization in parallel utilizing four modulators. Here a beamsplitter (BS) splits her light pulse into horizontal and vertical encoding paths. An amplitude modulator (AM) and phase modulation (PM) in each path allows encoding X_{ah} , P_{ah} , X_{av} , and P_{av} before using a half-wave plate with a 90° rotation and a polarizing beamsplitter (PBS) to recombine the encoded polarizations.

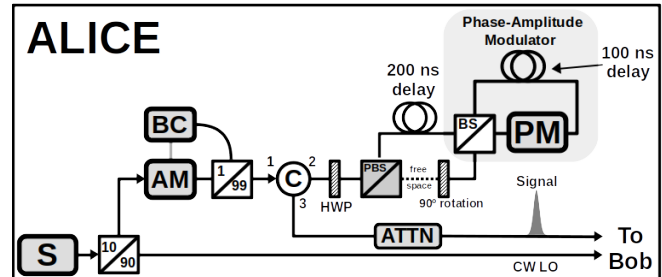


FIG. 4. Alice’s PA-CV-QKD transmitter consists of a laser source (S) split into a signal and LO path using a 10:90 beamsplitter (BS). The signal pulse is generated using an amplitude modulator (AM) and sent to port 1 of the circulator (C). Exiting port 2 of the circulator the optical power is balanced equally into polarization modes using an adjustable half-wave plate. A polarizing beamsplitter (PBS) sends horizontal (H) and vertical (V) polarizations along different paths (of different lengths) to the phase-amplitude modulator where distinct quadrature values are encoded to H and V . Encoded signals return to circulator port 2 and exit 3 to a final static attenuator (ATTN) before transmission to Bob. 10/90 \equiv 10:90 BS; BC \equiv bias controller; 1:99 \equiv 1:99 BS; HWP \equiv half-wave plate; PM \equiv phase modulator; CW \equiv continuous-wave; LO \equiv local oscillator

vibration environment [27], ms in a 68 km of aerial fiber [28], to minutes in 55 km of underground optical fiber [29]. Thus, the dataset used in parameter estimation should be adjusted accordingly. Clearly, parameter estimation will fail when the polarization changes approach the order of the signal repetition-rate. We note that polarization mode dispersion (PMD) is not typically relevant in current CVQKD systems due to their relatively slow operating speeds [28].

Bob’s receiver consists of an LO and at least one dual-quadrature homodyne detector (DQHD), a 90° optical hybrid (90OH), as seen in Fig. 5. For this proof-of-principle experiment we are using Alice’s laser as the LO, however a more secure method in a real deployment would be to utilize a true local oscillator [3, 30]. At the cost of an additional DQHD, Bob has the option of measuring in both polarizations to double the key rate. In this case Bob’s receiver would resemble a polarization di-

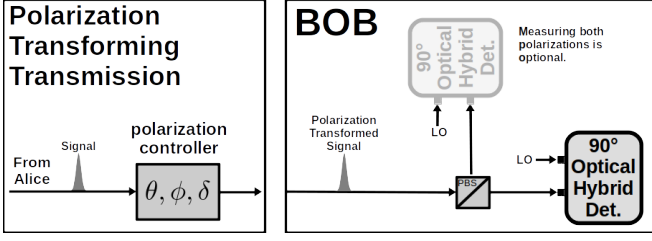


FIG. 5. Left) Between Alice and Bob we place a polarization controller to randomly change the polarization for each packet to simulate a real-world link. Right) Bob’s CV-QKD receiver consists of a polarizing beamsplitter (PBS) and at least one DQHD (a 90° optical hybrid detector). One can monitor both polarization modes to double the key-rate at the cost of an additional DQHD.

verse approach [9, 10], but for a given repetition rate we would have twice the key-rate. This doubling is due to having a unique GMCS CVQKD channel in each received polarization.

Bob measures all the pulses in a packet and extracts quadrature values X_{bh}, P_{bh} for each. Bob then sends Alice a portion of his measurements which Alice utilizes for parameter estimation. In this experiment, Bob shared 10% of his measured values. Utilizing a numerical least squares fitting algorithm [31] and the model given by Eq. 10 with terms such as those given in Eq. 11, the parameter estimation process recovers the transmission T , excess noise ξ , and the polarization parameters θ, ϕ , and δ .

To demonstrate our method we generated random polarization transformations (random θ, ϕ, δ) for each of 1000 packets. Since our proof-of-principle table-top experiment is assumed to have $T \approx 1$ over a short (40m) optical fiber link, we used a relatively low modulation variance $V_A = 1.16$, average photon number $\langle n \rangle = V_A/2 = 0.58$, to simulate real-world receiver side statistics. In Fig. 6 we give Poincaré spherical plots of the Stokes parameters given parameter estimates for δ and θ . Our Stokes parameters [32] are $S_1 = -\cos \delta \sin 2\theta$, $S_2 = \cos \delta \cos 2\theta$, and $S_3 = \sin \delta$. As seen in Fig. 6 our random transformations extend over the full range of possible values.

We use the R^2 value to characterize the correlations between Alice and Bob. In the case of our experiment this value is

$$R^2 = 1 - \frac{1}{N V_B} \sum_{i=1}^N \left(X_{Bi} - \frac{\eta T}{2} X_{Ai} \right)^2 \quad (16)$$

where $V_B = 1.32$, see Eq. 1, detector efficiency $\eta = 0.5$, transmission $T = 1$, excess noise $\xi = 0.0328$, and detector noise $\epsilon = 0.024$. It is straightforward to show that R^2 has maximum and minimum values

$$R_{\max}^2 = \frac{\eta T V_A}{2 V_B} = 0.219 \quad (17)$$

$$R_{\min}^2 = -\frac{\eta T V_A}{2 V_B} = -0.219. \quad (18)$$

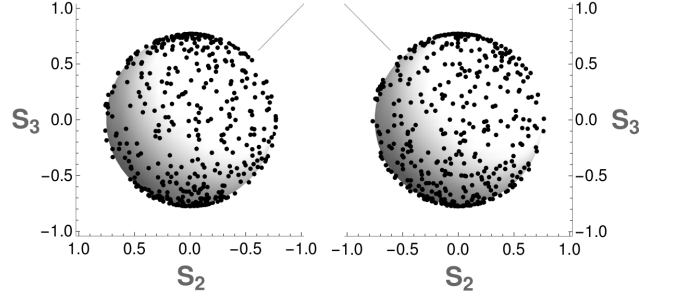


FIG. 6. Poincaré sphere representation of the Stokes parameters calculated using the polarization parameter estimates for δ and θ in our 1000 packet experiment. The parameter ϕ is a global phase and is ignored for this visualization. The left and right plots give opposite views of the sphere. The Stokes parameter S_1 is into the page.

In Fig. 7 we plot data for the correlation between Alice’s X_{ah} and Bob’s X_{bh} quadratures versus polarization parameter θ . Alice’s encodings have been corrected for phase for all cases with the determined ϕ and δ . The remaining parameter θ associated with the rotation given in Eq. 6 describes how much light rotates into the polarization orthogonal to a signal’s original encoding polarization. When $\theta = 0$ all signals stay in their original encoded polarization. For $\theta = \frac{\pi}{2}$ all light is rotated into the orthogonal polarization. In the case that Alice applies no θ correction to her stored encoding we find a correlation that decays with increasing θ reaching the predicted minimum at $\theta = \frac{\pi}{2}$. When Alice applies the correction for θ we measure a stable R^2 across all θ values with mean value $\langle R^2 \rangle = 0.214 \pm 0.005$, consistent with the expected value given in Eq 17.

A key element of our method is that it maintains a constant average photon number $\langle n \rangle = V_A/2$ from Alice even when polarization changes occur. This is important,

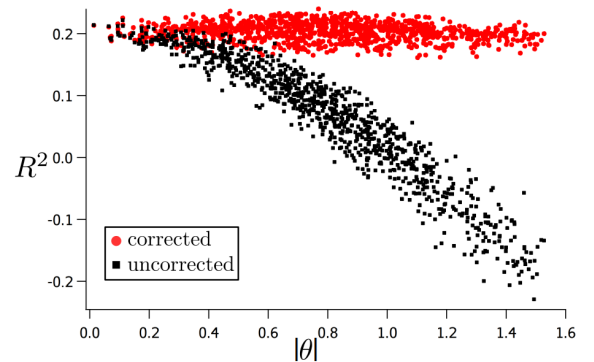


FIG. 7. R^2 correlation for X_{ah} and X_{bh} with and without rotating Alice’s encodings with the estimated θ value. As expected, a high correlation is achieved when full corrections are made to Alice’s encoding values. A decaying correlation is found when polarization rotations are ignored and not corrected.

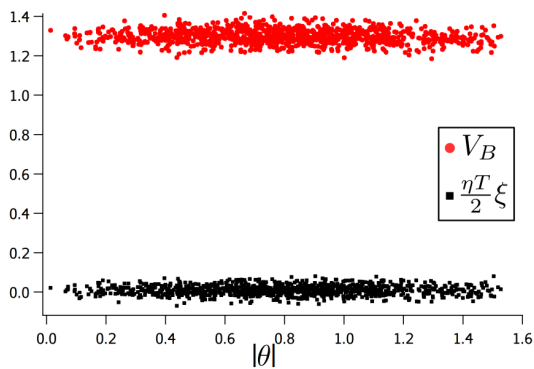


FIG. 8. Bob’s measured variance V_B and excess noise dependent quantity $\frac{\eta T}{2}\xi$ for quadrature X_{bh} . The V_B data suggests that the received signal strength is maintained regardless of polarization changes. Likewise, we see no polarization dependence in the excess noise ξ .

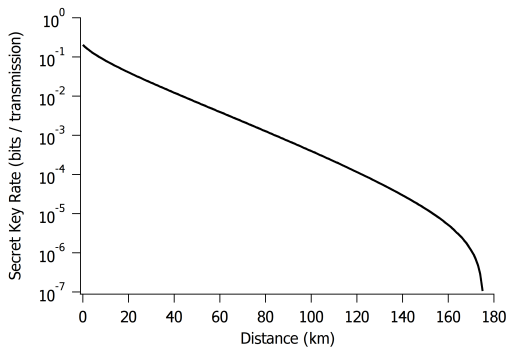


FIG. 9. Theoretical secret key-rate for the X_{ah} quadrature given the experimental parameters and $V_A = 1$ with an infinite key-length and trusted detector.

since the key rate is maximized for a given transmission T and excess noise ξ only when a specific V_A is utilized. Thus, the polarization changes impacting the signal will have no effect on the secret key-rate. As can be seen in Fig 8 Bob’s measured variance V_B , given in Eq. 1, is independent of the polarization rotation parameter θ . Similarly, we see no correlation in Bob’s excess noise η versus θ . This demonstrates that corrections to Alice’s stored encodings do not add polarization correction dependent noise which would manifest as excess noise. We note that the measured excess noise $\frac{\eta T}{2}\xi$ is plotted, key-rates are calculated using the noise we attribute to Eve which is the larger value ξ . The experimental excess noise from this data to be $\xi = 0.0328 \pm 0.003$ which is similar to our previous work with the same devices [3].

Given the measured excess noise $\xi = 0.0328$, detector

noise $\epsilon = 0.024$, detector efficiency $\eta = 0.5$, reconciliation efficiency $\beta = 0.95$, and fixed modulation variance $V_A = 1.16$, the secret-key rate prediction given an infinite key length and trusted detectors [33, 34] is given in Fig. 9. We note that finite-size effects should be considered in a real deployment as it sets a scale for how many final keys may be generated in a given time period for a given configuration [35].

IV. SECURITY IMPLICATIONS

While our method does introduce changes to Alice’s parameter estimation process there are no changes that alter the GMCS protocol [7]. We assume, as usual, that Eve has complete control of the polarization transformation occurring between Alice and Bob. She also knows the polarization parameters θ , ϕ , and δ exactly. This capability and knowledge does not give her any additional information about the GMCS raw or secret key. Once all parties know the polarization parameters and Alice transforms her stored encodings digitally, Alice, Bob, and Eve arrive at the standard GMCS scenario. In this case there are two GMCS channels in orthogonal polarizations, but they are completely independent.

V. DISCUSSION

We have presented a polarization agnostic encoding method for GMCS CVQKD. Our method removes the need to actively manipulate the optical signal to mitigate polarization changes in the optical link between Alice and Bob when monitoring a single polarization. In doing so, we eliminate the cost and loss associated with polarization control components. We also avoid noise injected by polarization correction algorithms. Future work will investigate real-world deployment of our method and integration of passive encoding methods [36, 37].

ACKNOWLEDGMENTS

This work was performed at Oak Ridge National Laboratory, operated by UT-Battelle for the U.S. Department of Energy under Contract No. DEAC05-00OR22725. Funding was provided by the U.S. Department of Energy under the Risk Management Tools and Technologies program in the Broadly Applicable Quantum Key Exchange Network (BAQKEN) project.

[1] E. Diamanti and A. Leverrier, *Entropy* **17**, 6072 (2015).
 [2] F. Laudenbach, C. Pacher, C.-H. F. Fung, A. Poppe, M. Peev, B. Schrenk, M. Hentschel, P. Walther, and

H. Hübel, *Advanced Quantum Technologies* **1**, 1800011 (2018).

- [3] B. P. Williams, B. Qi, M. Alshowkan, P. G. Evans, and N. A. Peters, *Physical Review Applied* **21**, 014056 (2024).
- [4] Y. Bian, Y. Pan, X. Xu, L. Zhao, Y. Li, W. Huang, L. Zhang, S. Yu, Y. Zhang, and B. Xu, *Applied Physics Letters* **124** (2024).
- [5] A. A. Hajomer, C. Bruynsteen, I. Derkach, N. Jain, A. Bomhals, S. Bastiaens, U. L. Andersen, X. Yin, and T. Gehring, *Optica* **11**, 1197 (2024).
- [6] Y. Piétri, L. Trigo Vidarte, M. Schiavon, L. Vivien, P. Grangier, A. Rhouni, and E. Diamanti, *Optica Quantum* **2**, 428 (2024).
- [7] F. Grosshans, G. Van Assche, J. Wenger, R. Brouri, N. J. Cerf, and P. Grangier, *Nature* **421**, 238 (2003).
- [8] Y. Zhang, Z. Chen, S. Pirandola, X. Wang, C. Zhou, B. Chu, Y. Zhao, B. Xu, S. Yu, and H. Guo, *Physical Review Letters* **125**, 010502 (2020).
- [9] D. Pereira, A. N. Pinto, and N. A. Silva, *Journal of Lightwave Technology* **41**, 432 (2023).
- [10] T. Wang, P. Huang, S. Wang, and G. Zeng, *Optics Express* **27**, 26689 (2019).
- [11] B. Chu, Y. Zhang, Y. Xu, and S. Yu, in *Conference on Lasers and Electro-Optics* (Optica Publishing Group, 2020) p. JTu2A.15.
- [12] Z. Tan, T. Wang, Y. Xu, X. Liu, L. Li, B. Zhang, Y. Liu, P. Huang, and G. Zeng, *Mathematics* **12**, 3599 (2024).
- [13] F. Roumestan, A. Ghazisaeidi, J. Renaudier, L. T. Vidarte, A. Leverrier, E. Diamanti, and P. Grangier, *Journal of Lightwave Technology* **42**, 5182 (2024).
- [14] W. Liu, Y. Cao, X. Wang, and Y. Li, *Physical Review A* **102**, 032625 (2020).
- [15] Y. Guo, X. Wang, L. Zhang, and D. Huang, *International Journal of Theoretical Physics* **58**, 209 (2019).
- [16] H. Wang, Y. Pi, W. Huang, Y. Li, Y. Shao, J. Yang, J. Liu, C. Zhang, Y. Zhang, and B. Xu, *Optics Express* **28**, 32882 (2020).
- [17] Y. Yamamoto and T. Kimura, *IEEE Journal of Quantum Electronics* **17**, 919 (1981).
- [18] K. Kikuchi, *Journal of Lightwave Technology* **34**, 157 (2015).
- [19] Misleadingly this has been referred to as a heterodyne detector in the CVQKD community. In the communications industry heterodyne detection refers to using an LO of a different frequency than the signal [38].
- [20] R. Loudon, *The quantum theory of light* (OUP Oxford, 2000).
- [21] G. D. VanWiggeren and R. Roy, *Applied Optics* **38**, 3888 (1999).
- [22] We note that this does not fully account for temporal effects of phenomenon such as polarization mode dispersion (PMD).
- [23] The relevant Jacobian is equal to 1.
- [24] M. Dennis, I. Duling, and W. Burns, *Electronics Letters* **32**, 547 (1996).
- [25] B. Qi and C. C. W. Lim, *Physical Review Applied* **9**, 054008 (2018).
- [26] H. Zhao, H. Li, Y. Xu, P. Huang, T. Wang, and G. Zeng, *Optics Letters* **47**, 2939 (2022).
- [27] P. M. Krummrich and K. Kotten, in *Optical Fiber Communication Conference* (Optica Publishing Group, 2004) p. F13.
- [28] R. Liu, H. Yu, J. Zan, S. Gao, L. Wang, M. Xu, J. Tao, J. Liu, Q. Chen, and Y. Zhao, *Optical Fiber Technology* **48**, 28 (2019).
- [29] P. Krummrich, E.-D. Schmidt, W. Weiershausen, and A. Mattheus, in *Optical Fiber Communication Conference* (Optica Publishing Group, 2005) p. OThT6.
- [30] B. Qi, P. Lougovski, R. Pooser, W. Grice, and M. Bobrek, *Physical Review X* **5**, 041009 (2015).
- [31] We used the C++ library Dlib, dlib.net.
- [32] E. Collett (Spie Bellingham, 2005).
- [33] J. Lodewyck, M. Bloch, R. García-Patrón, S. Fossier, E. Karpov, E. Diamanti, T. Debuisschert, N. J. Cerf, R. Tualle-Brouri, S. W. McLaughlin, *et al.*, *Physical Review A* **76**, 042305 (2007).
- [34] S. Fossier, E. Diamanti, T. Debuisschert, R. Tualle-Brouri, and P. Grangier, *Journal of Physics B: Atomic, Molecular and Optical Physics* **42**, 114014 (2009).
- [35] A. Leverrier, F. Grosshans, and P. Grangier, *Physical Review A* **81**, 062343 (2010).
- [36] B. Qi, P. G. Evans, and W. P. Grice, *Physical Review A* **97**, 012317 (2018).
- [37] B. Qi, H. Gunther, P. G. Evans, B. P. Williams, R. M. Camacho, and N. A. Peters, *Physical Review Applied* **13**, 054065 (2020).
- [38] H. H. Brunner, L. C. Comandar, F. Karinou, S. Bettelli, D. Hillerkuss, F. Fung, D. Wang, S. Mikroulis, Q. Yi, M. Kuschnerov, *et al.*, in *2017 19th international conference on transparent optical networks (ICTON)* (IEEE, 2017) pp. 1–4.